I&EC research
Industrial & Engineering Chemistry Research
pubs.acs.org/IECR
Article

Two-Binary-Interaction-Parameter Model for Molecular Solute + Ionic Liquid Solution

Lihang Bai, Tao Wang, Patricia B. Weisensee, Xiangyang Liu, and Maogang He*

Cite This: *Ind. Eng. Chem. Res.* 2021, 60, 11490−11501
Read Online

ABSTRACT: Ionic liquids are becoming increasingly important as environmentally friendly solvents for extraction and reactions. To describe the equilibrium phenomenon of monomolecular solute + ionic liquid, a two-binary-interaction-parameter (TBIP) model is proposed based on excess Gibbs free energy derived from excess internal energy, which circumvents the difficulty of directly formulating excessive entropy. Different from conventional binary solutions, monomolecular solute + ionic liquid is a peculiar ternary solution, which theoretically needs six binary-interaction parameters. However, due to strong repulsive electrostatic forces between like-ions, the like-ions pairs are negligible in comparison with dislike-ion and molecule−ion pairs. When local electroneutrality is assumed, the necessary binary interaction parameters finally are reduced to only two. Tested against experimental data, our TBIP model shows a better precision for most solutions than a non-random two-liquid (NRTL) model. When correlated with only half points, the TBIP model has a better extrapolation performance, while the NRTL model fails to work for R1234ze(E)/[EMIM][BF_4], ethanol/[MMIM][$(CH_3)_2PO_4$], and water/[EMIM][Tf_2N].

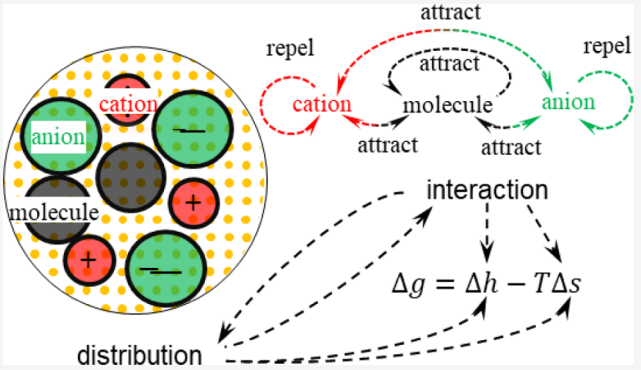

1. INTRODUCTION

Chemical process design and other industrial processes require phase equilibrium investigations. Broadly, practical methods are divided into equation-of-state methods and activity coefficient approaches.[1] Equation-of-state approaches predict volumetric and pressure data. Among equation-of-state methods, Soave−Redlich−Kwong (SRK) and Peng−Robinson (P−R) equations are the most significant, because they work well for both nonpolar and slight polar molecules.[2] Combining with mixing rules, equation-of-state models can derive phase equilibrium properties based on thermodynamic universal relations. Activity coefficient models are used to construct an excess Gibbs free energy function of compositional fractions. The universal quasi-chemical (UNIQUAC) equation is the most widely used model, especially for organic solutions. Based on UNIQUAC, a functional-group activity coefficient method was invented to predict equilibrium properties of new solutions without experiment data.[3−5] For electrolyte solutions, the Debye−Hückel theory is the best-known milestone on the way toward calculating activity coefficients, which focuses on electrostatic effects and extremely simplifies the calculation.[6−8] However, it was invented for solutions where the electrolyte concentration is small (mole fraction approaches zero).

As chemical engineering advances, ionic liquids (a new kind of solvent) are becoming increasingly important due to their tenability and chemical and thermal stabilities.[9−14] An ionic liquid is a kind of room-temperature molten salt, composed of cations and anions, with negligible vapor pressure. It is widely regarded as an environmentally friendly solvent for extraction and CO_2 capture.[15−20] However, there is a lack of specific thermodynamic models for ionic liquid solutions. Both P−R and SRK equations of state need an acentric factor, which is related to the boiling pressure.[3,21] However, since the ionic liquid has almost zero vapor pressure, it probably breaks down before it boils and at conditions much lower than the critical point parameters needed for the P−R and SRK equations of state. UNIQUAC models need extra structural parameters (van der Waals volume and area of the molecule relative to those of a standard segment).[22] Even for a ternary mixture, binary parameters are sufficient for UNIQUAC models. However, for ionic liquid solutions, six binary parameters are necessary due to the existence of three kinds of molecules (and ions). Even though Chen et al. altered the non-random two-liquid (NRTL) model to include strong electrostatic forces between ions and made it an electrolyte NRTL model (essentially a special non-random three-liquid model), the sizes of molecules and ions

Received: April 9, 2021
Revised: June 21, 2021
Accepted: June 28, 2021
Published: July 14, 2021

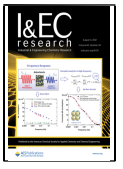

https://doi.org/10.1021/acs.iecr.1c01351
Ind. Eng. Chem. Res. 2021, 60, 11490−11501

were still neglected.[7,8] To cover long-range electrostatic forces, they combined the altered NRTL equation and Debye−Hückel theory. On the other hand, the combination repeatedly considered strong electrostatic interaction between ions.[23] The NRTL model was the first to consider local compositional heterogeneity. Due to its convenience, it is still widely adopted in chemical engineering including electrolyte solutions even though it ignores electrolytes' peculiar properties and molecules' sizes, highlighting that simplicity is a high priority in modeling.

To overcome the drawbacks of the aforementioned models, we propose a specific model for monomolecular solute + ionic liquid mixtures, which is self-consistent and fully covers the entropy effects. After simplification, we reduce the number of binary parameters to two. To evaluate the performance, the new model was experimentally tested against 19 different solutions and compared with to the NRTL model.

2. DERIVATION OF NEW MODEL

It is known that thermal properties at equilibrium can be derived from Gibbs energy based on the universal relations. The expression for excess Gibbs energy is given as

$$g^{\mathrm{E}} = h^{\mathrm{E}} - Ts^{\mathrm{E}} \approx a^{\mathrm{E}} = u^{\mathrm{E}} - Ts^{\mathrm{E}} \tag{1}$$

$$u^{\mathrm{E}} = -T^2 \frac{\partial}{\partial T}\left(\frac{a^{\mathrm{E}}}{T}\right) \tag{2}$$

First, we should note that the excess Gibbs energy g^{E} is composed of two terms: (1) excess enthalpy h^{E} (or energy part) caused by the new interaction between solvent and solute molecules; (2) excess entropy s^{E} caused by the new distribution of molecules and ions. The superscript E stands for "excessive" property values. For liquids, volume variation can be neglected, so g^{E} can be replaced by a Helmholtz free energy a^{E}, which is related to the internal energy u^{E}. Despite these simplifications, it is still too complicated to directly formulate s^{E}. Fortunately, s^{E} can be circumvented by an appropriate method. Here, we are building a model for liquid−liquid solutions, but it also works for gas−liquid solutions if one is interested in obtaining the fugacity for the gas components.[24] Due to the incompressibility of liquids and at moderate temperatures T,[25−27] the effect of excess volume v^{E} on g^{E} is negligible. As a result, g^{E} can be replaced by an excess Helmholtz free energy a^{E}. Followingly, we begin focusing on formulating a^{E}. From eq 2, a^{E} can be derived as

$$\begin{aligned} a^{\mathrm{E}} &= u^{\mathrm{E}} - T\int \frac{1}{T}\frac{\partial u^{\mathrm{E}}}{\partial T}\mathrm{d}T \\ &= u^{\mathrm{E}} - T\left[\frac{u^{\mathrm{E}}}{T}\right]_{T_0}^{T} + T\int_{T_0}^{T} u^{\mathrm{E}} d\left(\frac{1}{T}\right) \end{aligned} \tag{3}$$

Noticeably, u^{E}/T goes to zero when $T \to \infty$. In that case, eq 3 can be simplified to

$$a^{\mathrm{E}} = T\int_{\infty}^{T} u^{\mathrm{E}} d\left(\frac{1}{T}\right) \tag{4}$$

As of eq 4, we have not made any assumptions and it is theoretically correct. Meanwhile, eq 4 is an isovolumetric integral, which means there are no phase transitions or strong variations in u^{E}. Now, we need to find an expression with enough accuracy for the excess internal energy u^{E}. In the derivation of the NRTL model, u^{E} is adopted to cover local heterogeneity, as shown in eq 5.

$$u^{\mathrm{E}} = \frac{x_1 x_2 z N_{\mathrm{a}}}{2}\left[\frac{\varepsilon_1 \exp(-\varepsilon_1/k_{\mathrm{B}}T)}{x_1 + x_2 \exp(-\varepsilon_1/k_{\mathrm{B}}T)} + \frac{\varepsilon_2 \exp(-\varepsilon_2/k_{\mathrm{B}}T)}{x_2 + x_1 \exp(-\varepsilon_2/k_{\mathrm{B}}T)}\right] \tag{5}$$

$$\varepsilon_1 = \varepsilon_{21} - \varepsilon_{11} \qquad \varepsilon_2 = \varepsilon_{12} - \varepsilon_{22} \tag{6}$$

where ε_{11}, ε_{22}, and ε_{12} (ε_{21}) are the interactional energies between species 1 and species 1, species 2 and species 2, and species 1 and species 2, respectively, as shown in Figure 1. N_{a} is

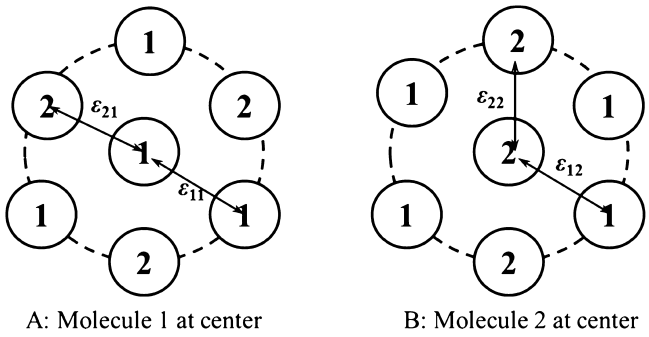

Figure 1. Schematic for the different interactions between molecules.

the Avogadro constant, and z is the coordination number (the number of adjacent molecules around the central molecule). Exemplarily, in Figure 1, $z = 6$. Essentially, z is correlated with the system dimension. For example, $z = 2$ in a one-dimensional Ising model. In a cubic lattice model, a molecule is immediately around by six molecules, hence $z = 6$.

We should notice that ε_{11} is asymptotic to a linear equation $y_{11} = a_{11}T + b_{11}$ when the temperature T is approaching infinity. Similarly, there exist asymptotes for ε_{22}, ε_{12}, and ε_{21}. Because molecules 1 and 2 both are spheres, it follows that $a_{11} = a_{12} = a_{21} = a_{22}$. Consequently, ε_1 and ε_1/T can be expressed like

$$\begin{aligned} &\frac{\varepsilon_1}{T} = a_{1,1}\beta + a_{1,2}\beta^2 + a_{1,3}\beta^3 + a_{1,4}\beta^4 \ldots \\ &\quad \text{where } \beta = \frac{1}{T} \text{ when } T \to \infty \end{aligned} \tag{7}$$

$$\varepsilon_1 = a_{1,1} + a_{1,2}\beta + a_{1,3}\beta^2 + a_{1,4}\beta^3 \ldots \qquad \text{when } T \to \infty \tag{8}$$

Similar to eqs 7 and 8, the same expressions for ε_2 and ε_2/T can be obtained. Substituting eq 5 into 4, a^{E} can be expressed as

$$a^{E} = \frac{x_1 x_2 N_a T}{2}\left[\begin{aligned} &\int_{\infty}^{T} \frac{\exp(-\varepsilon_1/k_{\mathrm{B}}T)}{x_1 + x_2 \exp(-\varepsilon_1/k_{\mathrm{B}}T)}\mathrm{d}\left(\frac{\varepsilon_1}{T}\right) \\ &\quad - \int_{\infty}^{T} \frac{1}{T}\frac{\exp(-\varepsilon_1/k_{\mathrm{B}}T)}{x_1 + x_2 \exp(-\varepsilon_1/k_{\mathrm{B}}T)}\mathrm{d}(\varepsilon_1) \\ &+ \int_{\infty}^{T} \frac{\exp(-\varepsilon_2/k_{\mathrm{B}}T)}{x_2 + x_1 \exp(-\varepsilon_2/k_{\mathrm{B}}T)}\mathrm{d}\left(\frac{\varepsilon_2}{T}\right) \\ &\quad - \int_{\infty}^{T} \frac{1}{T}\frac{\exp(-\varepsilon_2/k_{\mathrm{B}}T)}{x_2 + x_1 \exp(-\varepsilon_2/k_{\mathrm{B}}T)}\mathrm{d}(\varepsilon_2) \end{aligned}\right] \tag{9}$$

To accomplish the impossible integral in eq 9, Guggenheim postulated ε_1 and ε_2 are independent of temperature T.[28] In real applications, β is typically very small (<0.01) as the temperature

https://doi.org/10.1021/acs.iecr.1c01351
Ind. Eng. Chem. Res. 2021, 60, 11490−11501

T is usually above 200 K. So, when eqs 7 and 8 are substituted into eq 9, eq 9 will be equivalent to

$$a^{E} = \frac{x_1 x_2 N_a T}{2}\left[\begin{aligned}&\int_{\infty}^{T}\frac{\exp(-\varepsilon_1/k_BT)}{x_1 + x_2\exp(-\varepsilon_1/k_BT)}\mathrm{d}\left(\sum_{i=1}^{\infty}\alpha_{1,i}\beta^i - \sum_{i=2}^{\infty}\frac{i-1}{i}\alpha_{1,i}\beta^i\right)\\ &+\int_{\infty}^{T}\frac{\exp(-\varepsilon_2/k_BT)}{x_2 + x_1\exp(-\varepsilon_2/k_BT)}\mathrm{d}\left(\sum_{i=1}^{\infty}\alpha_{2,i}\beta^i - \sum_{i=2}^{\infty}\frac{i-1}{i}\alpha_{2,i}\beta^i\right)\end{aligned}\right] \tag{10}$$

As $\beta < 0.01$, the terms equal to or higher than β^2 are negligible. Finally, g^E can be expressed as

$$\begin{aligned} g^{E} &\approx a^{E}\\ &= -\frac{zRT}{2}\{x_1\ln[x_1 + x_2\exp(-\varepsilon_1/k_BT)] + x_2\\ &\quad \ln[x_2 + x_1\exp(-\varepsilon_2/k_BT)]\}\end{aligned} \tag{11}$$

With eq 11, g^E is obtained and covers the excess entropy effect. Although a similar expression of g^E has been published by Maurer and Prausnitz,[28] eq 10 is a more reasonable derivation to support the g^E expression and loosens the too restrictive conditions.

g^E is associated with activity coefficients γ like

$$g^{E} = RT(x_1\ln\gamma_1 + x_2\ln\gamma_2) \tag{12}$$

where R is the universal gas constant and x is a molar fraction. Subscripts 1 and 2 denote species #1 and #2, respectively. Misleading expressions of the activity coefficient, such as eqs 13 and 14 should be avoided. They cannot work for partially miscible solutions because they are monotonic functions with respect to solubility x.

$$\gamma_1 = \ln[x_1 + x_2\exp(-\varepsilon_1/kT)]^{-z/2} \tag{13}$$

$$\gamma_2 = \ln[x_2 + x_1\exp(-\varepsilon_2/kT)]^{-z/2} \tag{14}$$

According to the definition of thermodynamic potential, activity coefficients should instead be expressed as

$$\begin{aligned}\ln\gamma_1 = -\frac{z}{2}\Bigg\{&\ln[x_1 + x_2\exp(-\varepsilon_1/k_BT)]\\ &+ x_1x_2\frac{1-\exp(-\varepsilon_1/k_BT)}{x_1 + x_2\exp(-\varepsilon_1/k_BT)}\\ &- {x_2}^2\frac{1-\exp(-\varepsilon_2/k_BT)}{x_2 + x_1\exp(-\varepsilon_2/k_BT)}\Bigg\}\end{aligned} \tag{15}$$

$$\begin{aligned}\ln\gamma_2 = -\frac{z}{2}\Bigg\{&\ln[x_2 + x_1\exp(-\varepsilon_2/k_BT)]\\ &+ x_2x_1\frac{1-\exp(-\varepsilon_2/k_BT)}{x_2 + x_1\exp(-\varepsilon_2/k_BT)}\\ &- {x_1}^2\frac{1-\exp(-\varepsilon_1/k_BT)}{x_1 + x_2\exp(-\varepsilon_1/k_BT)}\Bigg\}\end{aligned} \tag{16}$$

Judging from eqs 15 and 16, the new model can work for partially miscible solutions, similar to the NRTL equation. To compare their characteristics, here, we studied Gibbs free energy variation Δg at different coordination numbers z when the interaction energy difference is set at $\varepsilon_1/k_BT = \varepsilon_2/k_BT = 1$. The results of two models are shown in Figures 2 and 3. The

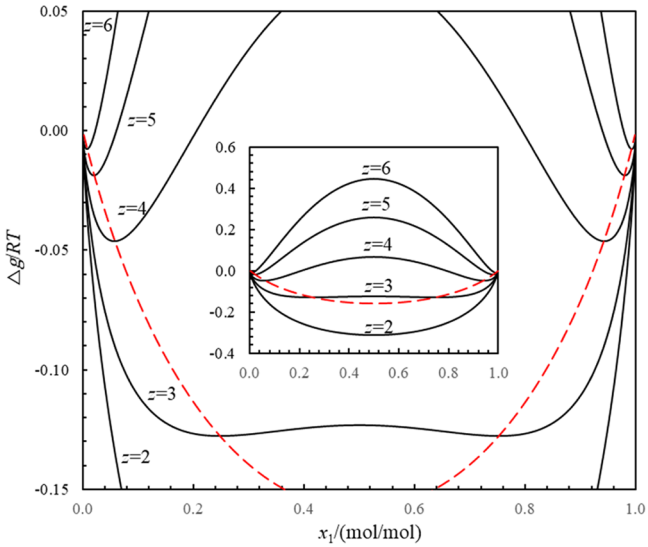

Figure 2. Gibbs free energy variation with respect to solubility for the new model.

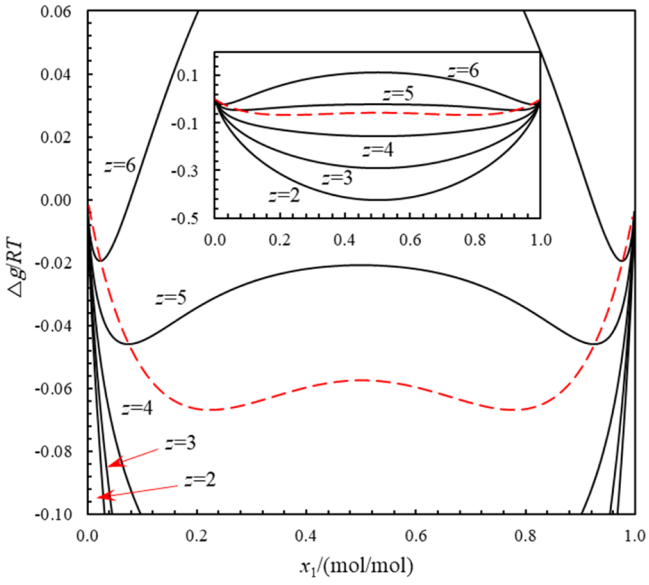

Figure 3. Gibbs free energy variation with respect to solubility for the NRTL model.

https://doi.org/10.1021/acs.iecr.1c01351
Ind. Eng. Chem. Res. 2021, 60, 11490−11501

comparison shows the new model has a lower Gibbs free energy than the NRTL model, because the NRTL model neglects entropy change. Additionally, the difference of Gibbs free energy between the two models increases with increasing z. Due to the models' symmetrical nature, phase separation occurs at the points, where $\frac{\partial}{\partial x_1}\left(\frac{\Delta g}{RT}\right) = 0$, which is intersected by the red dashed lines in Figures 2 and 3. From Figure 2, we see that phase separation begins at $z = 3$ for the new model, and $z = 5$ for the NRTL model. As we know, the one-dimensional Ising model does not have phase separation ($z = 2$). The two-dimensional Ising model ($z = 4$) includes phase separation, consistent with our two-binary-interaction-parameter (TBIP) model.

To investigate the new model further, we plot the relationship between z and ε_1/k_BT (ε_2/k_BT) at the respective equilibrium points in Figures 4 and 5. At a given z, for both models, increasing ε_1/k_BT leads to equilibrium at smaller x_1. Namely, increasing temperature leads to the equilibrium solubility x_1 approaching 0.5.

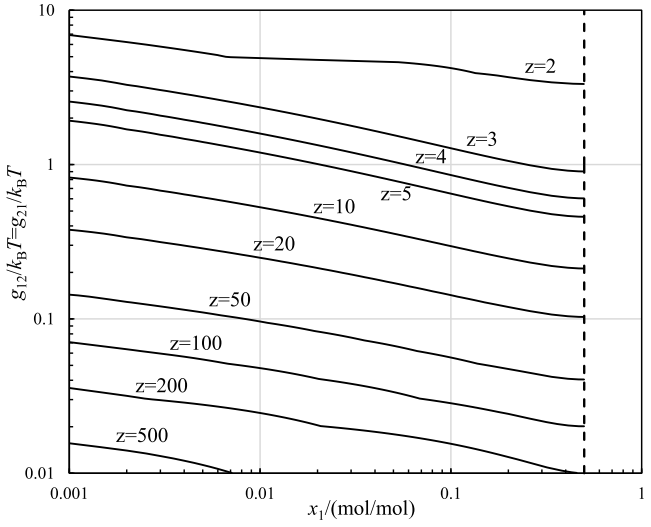

Figure 4. Parameter z of the new TBIP model at phase equilibrium.

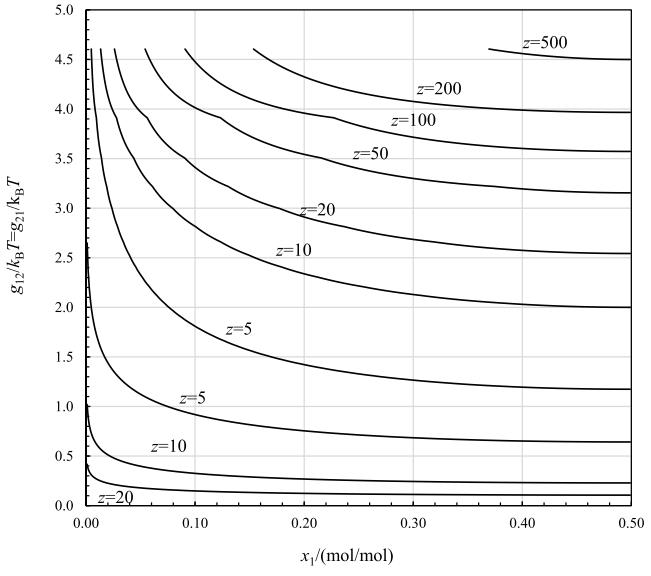

Figure 5. Parameter z of the NRTL model at phase equilibrium.

The difference of the two models stems from the relation between z and ε_1/k_BT. For the new model, at a given x_1, z decreases with reducing ε_1/k_BT and levels off around $z = 2$. A larger z means more interactional pairs with surrounding molecules, which amplifies the effect of $(\varepsilon_{11} - \varepsilon_{12})$ and $(\varepsilon_{22} - \varepsilon_{21})$. In the NRTL model, the variation of z becomes more complex with respect to ε_1/k_BT. With increasing ε_1/k_BT, z decreases first and then steeply goes up. To show it clearly, the comparison between the TBIP and NRTL models is given in Figure 6. To explain this unique phenomenon, we should focus

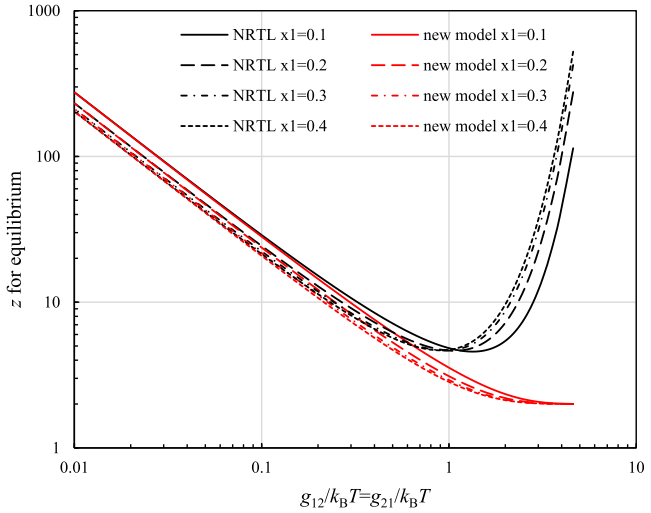

Figure 6. Comparison of z at phase equilibrium.

on the effect of ε_1 on Gibbs free energy $\Delta g = \Delta h - T\Delta s$. When $\varepsilon_1 = 0$, ε_1 has no effect on Δs. With increasing ε_1, the enthalpy Δh increases too, but Δs decreases and approaches zero, because large ε_1 and ε_2 reduce the probability of molecules #1 encountering molecules #2. Thus Δg will increase a little more than Δh. However, in the NRTL model, the effect of decreasing Δs is neglected. Thus Δg will still increase, but less than supposed. When ε_1 and ε_2 are large, Δg is significantly underestimated in the NRTL model. To accomplish phase separation, the NRTL model therefore needs a bigger coordination z to amplify the effect of ε_1 and ε_2.

3. ADJUSTMENT FOR SIZE DIFFERENCE

Generally, different molecules have different degrees of freedom, and ε_1/T and ε_2/T are not approaching zero at infinite temperature. So, the integral cannot be generally simplified as we did from eq 10 to 11. To satisfy eqs 7 and 8, we premise that a molecule's degree of freedom increases proportionally with its size (bigger molecules composed of more atoms have a higher degree of freedom). To evaluate molecular sizes, a volume element is introduced as shown in literature.[23] Thus, ε_{12} and ε_{21} in Figure 1 can be replaced with g_{12} and g_{21} in Figure 7. Similarly, g_1 and g_2 are approaching zero when T is approaching infinity. So, the integral can be simplified similar to eq 10 to 11. The excess Gibbs free energy and activity coefficients can then be states as shown in eqs 18−20.

$$g_1 = g_{21} - g_{11} \qquad g_2 = g_{12} - g_{22} \tag{17}$$

https://doi.org/10.1021/acs.iecr.1c01351
Ind. Eng. Chem. Res. 2021, 60, 11490−11501

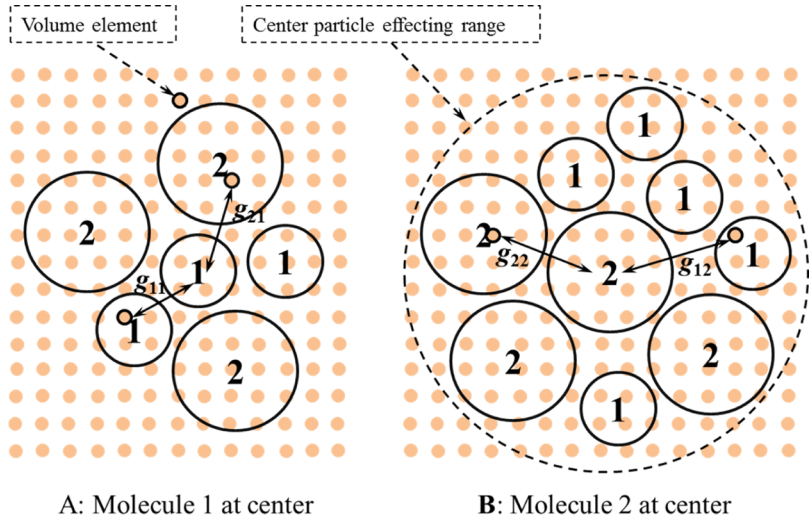

Figure 7. Local position in the different-size-particle solution.

$$g^{E} = -\frac{TR\lambda v}{2}\{\phi_1 \ln[\phi_1 + \phi_2 \exp(-g_1/kT)] + \phi_2 \ln[\phi_2 + \phi_1 \exp(-g_2/kT)]\} \quad (18)$$

$$\ln \gamma_1 = -\frac{\lambda}{2}\left\{\begin{aligned} &v_1 \ln[x_1v_1 + x_2v_2 \exp(-g_1/k_BT)] - v_1 \ln[x_1v_1 + x_2v_2] \\ &+ x_1v_1x_2\left[\frac{v_1 - v_2 \exp(-g_1/k_BT)}{x_1v_1 + x_2v_2 \exp(-g_1/k_BT)} - \frac{v_1 - v_2}{x_1v_1 + x_2v_2}\right] \\ &- {x_2}^2v_2\left[\frac{v_2 - v_1 \exp(-g_2/k_BT)}{x_2v_2 + x_1v_1 \exp(-g_2/k_BT)} - \frac{v_2 - v_1}{x_2v_2 + x_1v_1}\right] \end{aligned}\right\} \quad (19)$$

$$\ln \gamma_2 = -\frac{\lambda}{2}\left\{\begin{aligned} &v_2 \ln[x_2v_2 + x_1v_1 \exp(-g_2/k_BT)] - v_2 \ln[x_2v_2 + x_1v_1] \\ &+ x_1v_2x_2\left[\frac{v_2 - v_1 \exp(-g_2/k_BT)}{x_2v_2 + x_1v_1 \exp(-g_2/k_BT)} - \frac{v_2 - v_1}{x_2v_2 + x_1v_1}\right] \\ &- {x_1}^2v_1\left[\frac{v_1 - v_2 \exp(-g_1/k_BT)}{x_1v_1 + x_2v_2\exp(-g_1/k_BT)} - \frac{v_1 - v_2}{x_1v_1 + x_2v_2}\right] \end{aligned}\right\} \quad (20)$$

where ϕ is the volume fraction of the different compositions, and v and λ are the molar volume of the solution and a constant coefficient, respectively. Comparing with (11), g^E in eq 18 depends on the solution volume and the volumes of the pure substances. With large molecules, the variation of g^E is substantial.

4. ADJUSTMENT FOR IONIC LIQUIDS

As is well known, ionic liquids contain at least two kinds of ions (cation and anion). When a molecular gas is dissolved in an ionic liquid, there will be three kinds of molecules (or ions) in the solution, which resembles a ternary mixture. Actually, ionic liquid solutions have their own peculiar characteristics different from conventional ternary mixtures. Due to strong repulsive forces between like-ions, the pairs of cation−cation and anion−anion are negligible,[6,8,23] which means there exist only g_{11}, g_{21}, g_{31}, g_{12}, g_{32}, and g_{23} (1: molecule, 2: anion, 3: cation). Additionally, local electroneutrality leads to[7,8]

$$g_{21} = g_{31} \quad (21)$$

$$(g_{12} - g_{32})/(g_{13} - g_{23}) = v_2/v_3 \quad (22)$$

According to our previous work, excess internal energy u^E can be expressed by eq 23.[23] Consequently, we can get the excess Gibbs free energy in eq 24 and activity coefficient in eqs 25 and 26 when only considering the energy effect.

https://doi.org/10.1021/acs.iecr.1c01351
Ind. Eng. Chem. Res. 2021, 60, 11490−11501

$$u^{E} = \frac{\lambda N_a}{2}\left\{\begin{array}{l} x_1 v_1 (g_{21} - g_{11}) \dfrac{x_2 v_2 \exp\left(-\frac{g_{21}-g_{11}}{k_B T}\right) + x_3 v_3 \exp\left(\frac{g_{31}-g_{11}}{k_B T}\right)}{x_1 v_1 + x_2 v_2 \exp\left(-\frac{g_{21}-g_{11}}{k_B T}\right) + x_3 v_3 \exp\left(-\frac{g_{31}-g_{11}}{k_B T}\right)} \\ + x_2 v_2 (g_{12} - g_{32}) \dfrac{x_1 v_1 \exp\left(-\frac{g_{12}-g_{32}}{k_B T}\right)}{x_1 v_1 \exp\left(-\frac{g_{12}-g_{32}}{k_B T}\right) + x_3 v_3} \\ + x_3 v_3 \dfrac{v_3}{v_2} (g_{12} - g_{32}) \dfrac{x_1 v_1 \exp\left(-\frac{v_3 g_{12}-g_{32}}{v_2 k_B T}\right)}{x_1 v_1 \exp\left(-\frac{v_3 g_{12}-g_{32}}{v_2 k_B T}\right) + x_2 v_2} \end{array}\right\} \tag{23}$$

$$g^{E} = \frac{-k\lambda N_a}{2}\left\{\begin{array}{l} x_1 v_1 \ln\left[x_1 v_1 + (x_2 v_2 + x_3 v_3)\exp\left(-\dfrac{g_{21} - g_{11}}{k_B T}\right)\right] - x_1 v_1 \ln[x_1 v_1 + x_2 v_2 + x_3 v_3] \\ + x_2 v_2 \ln\left[x_1 v_1 \exp\left(-\dfrac{g_{12} - g_{32}}{k_B T}\right) + x_3 v_3\right] - x_2 v_2 \ln[x_1 v_1 + x_3 v_3] \\ + x_3 v_3 \ln\left[x_1 v_1 \exp\left(-\dfrac{v_3}{v_2}\dfrac{g_{12} - g_{32}}{k_B T}\right) + x_2 v_2\right] - x_3 v_3 \ln[x_1 v_1 + x_2 v_2] \end{array}\right\} \tag{24}$$

$$\ln \gamma_1 = \frac{-\lambda}{2}\left\{\begin{array}{l} v_1 \ln\left[x_1 v_1 + x_2 (v_2 + v_3)\exp\left(-\dfrac{g_{21} - g_{11}}{k_B T}\right)\right] - v_1 \ln[x_1 v_1 + x_2 (v_2 + v_3)] \\ + x_1 x_2 v_1 \left[\dfrac{v_1 - (v_2 + v_2)\exp\left(-\frac{g_{21}-g_{11}}{k_B T}\right)}{x_1 + x_2 (v_2 + v_3)\exp\left(-\frac{g_{21}-g_{11}}{k_B T}\right)} - \dfrac{v_1 - (v_2 + v_3)}{x_1 + x_2 (v_2 + v_3)}\right] \\ + x_2 x_2 v_2 \left[\dfrac{v_1 \exp\left(-\frac{g_{12}-g_{32}}{k_B T}\right) - v_3}{x_1 \exp\left(-\frac{g_{12}-g_{32}}{k_B T}\right) + x_3 v_3} - \dfrac{v_1 - v_3}{x_1 + x_3 v_3}\right] \\ + x_3 x_3 v_3 \left[\dfrac{v_1 \exp\left(-\frac{v_3}{v_2}\frac{g_{12}-g_{32}}{k_B T}\right) - v_2}{x_1 \exp\left(-\frac{v_3}{v_2}\frac{g_{12}-g_{32}}{k_B T}\right) + x_2 v_2} - \dfrac{v_1 - v_2}{x_1 + x_2 v_2}\right] \end{array}\right\} \tag{25}$$

https://doi.org/10.1021/acs.iecr.1c01351
Ind. Eng. Chem. Res. 2021, 60, 11490−11501

$$\ln \gamma_1 = \frac{-\lambda}{2}\left\{\begin{array}{l} \nu_2 \ln\left[x_1\nu_1 \exp\left(-\frac{g_{12}-g_{32}}{k_B T}\right) + x_3\nu_3\right] - \nu_2 \ln[x_1\nu_1 + x_3\nu_3] \\ + \nu_3 \ln\left[x_1\nu_1 \exp\left(-\frac{\nu_3}{\nu_2}\frac{g_{12}-g_{32}}{k_B T}\right) + x_2\nu_2\right] - \nu_3 \ln[x_1\nu_1 + x_2\nu_2] \\ + x_1x_2\nu_2\left[\frac{-\nu_1 \exp\left(-\frac{g_{12}-g_{32}}{k_B T}\right) + \nu_3}{x_1\nu_1 \exp\left(-\frac{g_{12}-g_{32}}{k_B T}\right) + x_3\nu_3} - \frac{-\nu_1+\nu_3}{x_1+\nu_1+x_3\nu_3}\right] \\ + x_1x_3\nu_3\left[\frac{-\nu_1 \exp\left(-\frac{\nu_3}{\nu_2}\frac{g_{12}-g_{32}}{k_B T}\right) - \nu_2}{x_1\nu_1 \exp\left(-\frac{\nu_3}{\nu_2}\frac{g_{12}-g_{32}}{k_B T}\right) + x_2\nu_2} - \frac{-\nu_1+\nu_2}{x_1+\nu_1+x_2\nu_2}\right] \\ + x_1x_1\nu_1\left[\frac{-\nu_1 + (\nu_2+\nu_3)\exp\left(-\frac{g_{12}-g_{32}}{k_B T}\right)}{x_1\nu_1 + x_2(\nu_2+\nu_3) + \exp\left(-\frac{g_{12}-g_{32}}{k_B T}\right)} - \frac{-\nu_1+(\nu_2+\nu_3)}{x_1+x_2(\nu_2+\nu_3)}\right] \end{array}\right\} \quad (26)$$

where λ denotes the ratio of molecular volume to the volume of the volume element, namely, a constant parameter for the new model.

5. CONFIGURATIONAL ENTROPY

In addition to the energy effect, molecular structure also influences entropy and thus Gibbs free energy. In this field, the Huggins−Flory method has inspired many researchers.[29] The Huggins−Flory method was proposed for chain polymer solutions, which covered not only molecular sizes but also polymer deformations. For example, solvophilic polymers will spread in solutions while solvophobic polymer will twist into a ball. However, this method is not applicable to molecules containing rings.[22,30] Unlike polymer chains, organic vapors and ionic liquids are relatively short and are not so flexible as polymer chains. Ionic liquids are also different from conventional liquids, composed of at least two kinds of ions and having strong interactions between ions. These special characteristics should be considered for entropy change. According to the Flory−Huggins theory, the allocation number for the first molecule is

$$n_1 = N_r z(z-1)^{r-2} \quad (27)$$

where N_r is the total liquid lattice number, z is still the coordination number, and r is the segment number for a molecule. In Flory−Huggins' theory, each segment occupies one of the lattices. To some extent, the segment plays the same role as the volume element in Figure 7. For the ith molecule, the allocation number is

$$n_i = [N_r - (i-1)r]z\frac{N_r-(i-1)r}{N_r}\left[(z-1)\frac{N_r-(i-1)r}{N_r}\right]^{r-2} \quad (28)$$

If the molecule is not a long chain and has no flexibility, the allocation number for ith molecule can be simplified to

$$n_i = N_r - (i-1)r \quad (29)$$

Obviously, eq 28 neglects the azimuthal difference of the ith molecule. In dense liquids, all ions and molecules are not spherical and their orientation is strongly determined by surrounding species. Since orientational distribution has been covered by considering a spatial distribution, orientational distribution should not be repeatedly considered in eq 28. Finally, we have the entropy change for an athermal solution.

$$\Delta s = k \ln \frac{\Omega_{solu}}{\Omega_1\Omega_2} = k \ln \frac{\frac{1}{r_1^{-N_1}}\frac{(N_r/r_1)!}{(N_r/r_1-N_1)!}\frac{1}{r_2^{-N_2}}\frac{[(N_r-N_1r_1)/r_2]!}{[(N_r-N_1r_1-N_2r_2)/r_2]!}\frac{1}{r_3^{-N_3}}N_3!}{\frac{1}{r_2^{-N_2}}\frac{[(N_2r_2+N_3r_3)/r_2]!}{(N_3r_3/r_2)!}\frac{N_3!}{r_3^{-N_3}} \times \frac{N_1!}{r_1^{-N_1}}} = -x_1R \ln \phi_1 - x_2\frac{r_3+r_2}{r_1}R \ln \phi_2 \quad (30)$$

Expression 29 does not consider strong repulsive and dragging forces between ions. When considering the ions' strong interactions, the allocation numbers will decrease significantly, but it still gives the same result, because the terms for ions in the numerator and denominator would be reduced. Using eq 30, the configurational entropy variation is obtained. If neglecting molecular size (or ions) effects, eq 30 can be expressed as

$$\Delta s = -x_1R \ln x_1 - x_2R \ln x_2 \quad (31)$$

The expression in eq 31 is the same as for an ideal binary mixture, which explains why ionic liquid solutions can be regarded as standard solutions and NRTL models can be widely adopted for ionic liquid solutions despite them being ternary mixtures.

Combining the interaction effect and configuration variation, excess Gibbs free energy and activity coefficients are expressed, respectively, by

https://doi.org/10.1021/acs.iecr.1c01351
Ind. Eng. Chem. Res. 2021, 60, 11490−11501

$$\frac{g^{E}}{RT} = \frac{-\lambda}{2}\left\{\begin{array}{l} x_1\nu_1 \ln\left[x_1\nu_1 + (x_2\nu_2 + x_3\nu_3)\exp\left(-\frac{g_{21}-g_{11}}{kT}\right)\right] \\ \quad - x_1\nu_1 \ln[x_1\nu_1 + x_2\nu_2 + x_3\nu_3] \\ + x_2\nu_2 \ln\left[x_1\nu_1 \exp\left(-\frac{g_{12}-g_{32}}{kT}\right) + x_3\nu_3\right] \\ \quad - x_2\nu_2 \ln[x_1\nu_1 + x_3\nu_3] \\ + x_3\nu_3 \ln\left[x_1\nu_1 \exp\left(-\frac{\nu_3}{\nu_2}\frac{g_{12}-g_{32}}{kT}\right) + x_2\nu_2\right] \\ \quad - x_3\nu_3 \ln[x_1\nu_1 + x_2\nu_2] \end{array}\right\} + x_1 \ln\frac{x_1\nu_1}{x_1\nu_1 + x_2(\nu_2+\nu_3)} + x_2\frac{\nu_3+\nu_2}{\nu_1}\ln\frac{x_2(\nu_2+\nu_3)}{x_1\nu_1 + x_2(\nu_2+\nu_3)} - x_1 \ln x_1 - x_2 \ln x_2 \tag{32}$$

$$\ln\gamma_1 = \frac{-\lambda}{2}\left\{\begin{array}{l} \nu_1 \ln\left[x_1\nu_1 + x_2(\nu_2+\nu_3)\exp\left(-\frac{g_{21}-g_{11}}{kT}\right)\right] - \nu_1 \ln[x_1\nu_1 + x_2(\nu_2+\nu_3)] \\ + x_1x_2\nu_1\left[\frac{\nu_1 - (\nu_2+\nu_3)\exp\left(-\frac{g_{21}-g_{11}}{kT}\right)}{x_1\nu_1 + x_2(\nu_2+\nu_3)\exp\left(-\frac{g_{21}-g_{11}}{kT}\right)} - \frac{\nu_1-(\nu_2+\nu_3)}{x_1 + x_2(\nu_2+\nu_3)}\right] \\ + x_2x_2\nu_2\left[\frac{\nu_1\exp\left(-\frac{g_{21}-g_{11}}{kT}\right) - \nu_3}{x_1\nu_1\exp\left(-\frac{g_{21}-g_{11}}{kT}\right) + x_3\nu_3} - \frac{\nu_1-\nu_3}{x_1+x_3\nu_3}\right] \\ + x_3x_3\nu_3\left[\frac{\nu_1\exp\left(-\frac{g_{21}-g_{11}}{kT}\right) - \nu_2}{x_1\nu_1\exp\left(-\frac{g_{21}-g_{11}}{kT}\right) + x_2\nu_2} - \frac{\nu_1-\nu_2}{x_1+x_2\nu_2}\right] \end{array}\right\} + \ln\frac{\nu_1}{x_1\nu_1 + x_2(\nu_2+\nu_3)} \tag{33}$$

$$\ln\gamma_2 = \frac{-\lambda}{2}\left\{\begin{array}{l} \nu_2 \ln\left[x_1\nu_1\exp\left(-\frac{g_{21}-g_{11}}{kT}\right) + x_3\nu_3\right] - \nu_2\ln[x_1\nu_1 + x_3\nu_3] \\ \nu_3 \ln\left[x_1\nu_1\exp\left(-\frac{\nu_3}{\nu_2}\frac{g_{21}-g_{11}}{kT}\right) + x_2\nu_2\right] - \nu_3\ln[x_1\nu_1 + x_2\nu_2] \\ + x_2x_2\nu_2\left[\frac{-\nu_1\exp\left(-\frac{g_{21}-g_{11}}{kT}\right) + \nu_3}{x_1\nu_1\exp\left(-\frac{g_{21}-g_{11}}{kT}\right) + x_3\nu_3} - \frac{-\nu_1+\nu_3}{x_1+\nu_1+x_3\nu_3}\right] \\ + x_1x_3\nu_3\left[\frac{-\nu_1\exp\left(-\frac{g_{21}-g_{11}}{kT}\right) + \nu_2}{x_1\nu_1\exp\left(-\frac{\nu_3}{\nu_2}\frac{g_{21}-g_{11}}{kT}\right) + x_2\nu_2} - \frac{-\nu_1+\nu_2}{x_1+\nu_1+x_2\nu_2}\right] \\ + x_1x_1\nu_1\left[\frac{-\nu_1 + (\nu_2+\nu_3)\exp\left(-\frac{g_{21}-g_{11}}{kT}\right)}{x_1\nu_1 + x_2(\nu_2+\nu_3)\exp\left(-\frac{g_{21}-g_{11}}{kT}\right)} - \frac{-\nu_1+(\nu_2+\nu_3)}{x_1+x_2(\nu_2+\nu_3)}\right] \end{array}\right\} + \frac{\nu_1\nu_3}{\nu_1}\ln\frac{x_2(\nu_2+\nu_3)}{x_1\nu_1 + x_2(\nu_2+\nu_3)}\ln x_\partial \tag{34}$$

where $(g_{21} - g_{11})$ and $(g_{12} - g_{32})$ are only two parameters for binary interactions. The new model is thus named as the two

https://doi.org/10.1021/acs.iecr.1c01351
Ind. Eng. Chem. Res. 2021, 60, 11490−11501

Table 1. Parameters and Deviations of the TBIP Model for 19 Solutions[a]

solution	A	τ_1	τ_2	τ_3	τ_4	1000 × AAD[a]
R152a/[P(14)666][TMPP][34,35]	0.014	1.38×10^5	-2.91×10^7	-6.63×10^3	2.25×10^6	2.6
R245fa/[P(14)666][TPMM][34,35]	43.591	-1.18×10^3	1.54×10^5	8.27	2.47×10^3	1.9
R227ea/[P(14)666][TPMM][34,35]	−1.366	-4.96×10^2	1.38×10^5	-2.26×10^9	5.73×10^{-1}	2.7
R1234ze(E)/[Emim][BF_4][36,37]	1.475	3.52×10	8.95×10^4	5.11×10^2	-1.49×10^5	0.9
R1234ze(E)/[Hmim][BF_4][36,37]	0.462	1.89×10^3	-2.86×10^5	2.97×10^2	-7.85×10^4	1.4
R1234ze(E)/[Omim][BF_4][36,37]	0.709	1.01×10^3	-1.21×10^5	2.47×10^3	-6.54×10^4	1.5
R134a/[P(14)666][TMPP][35,38]	0.657	-9.27×10^2	5.08×10^5	-1.60×10^6	-7.88×10^5	5.5
R134a/[P(14)666][TMPP][35,38]	0.311	2.34×10^3	4.30×10^4	2.11×10^3	1.24	3.5
R134a/[P(14)666][TMPP][35,38]	0.062	1.21×10^3	1.74×10^6	-1.55×10^6	-5.08×10^5	2.7
R32/[dmpim][TMeM][39]	0.803	8.32×10^2	-1.32×10^5	2.11×10^3	3.09×10^4	2.2
R32/[emim][BEI][39,40]	0.723	6.78×10^2	-8.06×10^4	-8.76×10	1.44×10^4	3.3
R32/[emim][BMeI][39,41]	0.990	6.56×10^2	-9.09×10^4	-1.39×10^2	1.42×10^4	1.9
R32/[pmpy][BMeI][39,42]	0.995	1.23×10^3	-2.40×10^5	-6.45×10^2	1.41×10^5	3.0
SO_2/[hmim][Tf_2N][43,44]	−0.792	-2.57×10^2	6.83×10^4	7.96×10^2	-2.65×10^6	11.5
water/choline glycolate[45,46]	−1.144	-2.53×10^2	1.84×10^5	-1.60×10^4	-3.82×10	13.7
water/choline lactate[45,47]	−0.547	2.07×10^3	-7.33×10^5	-9.32×10^4	5.28	5.9
ethanol/[MMIM][$(CH_3)_2PO_4$][47,48]	−2.252	-7.84×10^2	1.41×10^2	1.39	6.78×10^4	6.5
acetone/[MMIM][$(CH_3)_2PO_4$][47,48]	46.765	8.05×10	4.17	-2.96×10^2	−1.66	4.2
water/[emim][tf_2n][49,50]	−2.597	-1.62×10^3	2.80×10^5	2.26×10^5	-7.32×10^7	3.9

[a]AAD (average absolute deviation) = $\sum|x_{cal} - x_{exp}|/n$.

binary-interaction-parameter (TBIP) model. For convenience, the TBIP model uses five parameters (α, τ_1, τ_2, τ_3, and τ_4) to fit with the experimental data, similar to the NRTL model

$$\frac{-\lambda v_1}{2} = \alpha \tag{35}$$

$$g_{21} - g_{11} = \tau_1 + \tau_2/T \tag{36}$$

$$g_{12} - g_{32} = \tau_3 + \tau_4/T \tag{37}$$

6. PERFORMANCE OF THE NEW MODEL

Since the TBIP model is non-symmetrical, it is inconvenient to analyze its performance at a specific γ^∞ by assuming several parameters. To test its performance, we used the TBIP model to correlate it with experimental data and evaluate its precision and robustness. When the solution reaches equilibrium, the following equation is met.[31,32]

$$y_i p \Phi_i = x_i \gamma_i p_i^s \tag{38}$$

$$\Phi_i = \exp\left[\frac{(B_i - v_i^l)(p - p_i^s)}{RT}\right] \tag{39}$$

where x_i and y_i are the mole fraction of ith species in the solution and in the gas phase, respectively. B_i and v_i are the second viral factor and the molar volume and partial volume of ith species, respectively, and p^s and γ_i are saturation pressure and activity coefficient of ith species, respectively. Here, we tested the TBIP model with 19 different types of typical molecular solute/ionic liquid solutions, as shown in Table 1. In the correlation, thermal properties of the solutes were calculated with the software REFPROP 9.1.[33] Some of these solutions are partially miscible, some totally miscible. Some have big molecules, while some have big cations or anions. To evaluate the performance, the deviations were compared to that of the NRTL model in Table S1.

When fitted with all the data, we obtain the results, as shown in Figure 8. We can see that when fitted to the entire data set,

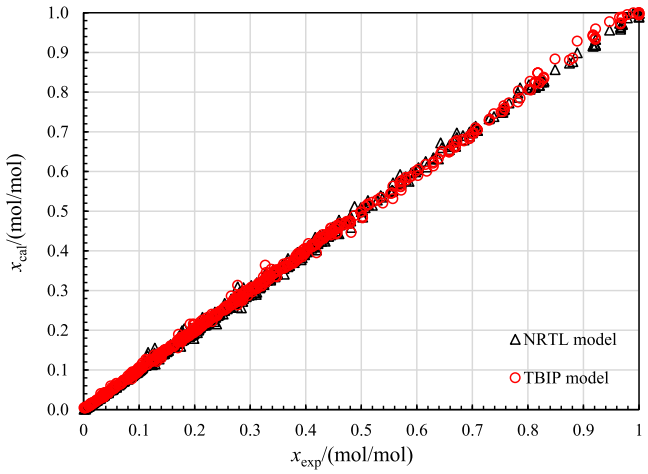

Figure 8. TBIP and NRTL model comparison when fitting with all data (x (molecular solute) + (1 − x) (ionic liquid)).

both TBIP and NRTL models work well. According to Table S1, the worst prediction of the TBIP model occurs for ethanol/[MMIM][$(CH_3)_2PO_4$] (AAD (average absolute deviation, see Table 1) = 0.0137 mol/mol, MAD (maximum absolute deviation, see Table 1) = 0.0394 mol/mol) and water/choline lactate (AAD = 0.0115 mol/mol and MAD = 0.0357 mol/mol). The big deviations may be caused by the unreliability of those experimental data. It should be noted that all experimental data have a specific uncertainty. In Table 2, some uncertainties and measurement conditions are compared. Unfortunately, the solubility uncertainty of ethanol/[MMIM][$(CH_3)_2PO_4$] was not stated in the paper. It can also be doubted that such a highly precise thermometer (uncertainty = 0.001 K) matches with a low-quality pressure sensor (reproducibility = 0.005% of the maximum pressure 350 kPa). Although the solubility uncertainty of water/choline lactate and water/choline glycolate was given by the authors, it was calculated only based on the microbalance uncertainty but neglected the impurities of the ionic liquids. Generally, ionic liquids have impurities far beyond

https://doi.org/10.1021/acs.iecr.1c01351
Ind. Eng. Chem. Res. 2021, 60, 11490−11501

Table 2. Uncertainties (u_T, u_p and u_x) and Experimental Conditions of Solubility Measurement

	u_T/K	u_p/Pa	u_x/(mol/mol)	T/K	p/kPa	x/(mol/mol)
water/choline lactate	0.05	160	0.0001[a]	293.15−323.15	0.22−12.34	0.197−1
water/choline glycolate	0.05	160	0.0001[a]	293.15−323.15	0.12−12.34	0.327−1
ethanol/[MMIM][$(CH_3)_2PO_4$]	0.001[b]	17.5[c]		353.15	0.66−182.61	0.107−1
water/[EMIM][Tf_2N]	0.018	1	0.0004	292.75−323.35	1.82−9.56	0.115−0.311

[a]Calculated only based on microbalance uncertainty but neglecting impurities, so unreliable. [b]Unbelievable for a Pt-100 sensor, may be a typo mistake by the author. [c]Reproducibility other than true uncertainty, maybe $u_p \approx 175$ Pa.

0.0001 mol/mol due to their hygroscopicity. For low vapor pressure solutes, pressure uncertainty poses a non-trivial impact on activity coefficient calculations. From eq 38, the relative uncertainty of the activity coefficient induced by pressure uncertainty can be expressed as

$$\frac{\Delta\gamma_1}{\gamma_1} = \frac{\Delta p}{p} \tag{40}$$

Obviously, at low pressure, the relative uncertainty of the activity coefficient is susceptible. In actual experiments, due to low saturation pressure of ethanol and water, ethanol/[MMIM][$(CH_3)_2PO_4$] and water/choline lactate pressures are prone to larger uncertainties. In the apparatus measuring water/choline lactate, the uncertainty of the pressure transducer was 800 Pa as given by the provider or 160 Pa, as stated by the author.[47] Consequently, among the solubility points of water/choline lactate, the biggest pressure uncertainty is 72.7%, and half thereof over 6.58%. Solubility of water/[emim][Tf_2N] was determined with a reliable apparatus. Our TBIP model works better than the NRTL model for this water/[emim][Tf_2N] mixture.

To compare the robustness, we also fitted the models with only the lower half solubility points to obtain the parameters and then used these parameters to predict all solubilities. The results are shown in Figure 9. The TBIP model still works well, while the NRTL model fails for R1234ze(E)/[EMIM][BF_4]. Nine out of 19 types of solutions have an AAD below 0.005 for the TBIP model, compared to five out of 19 solutions for the NRTL model. Figure 10 shows the results when fitted only with the upper half. Comparing with Figure 9, it is found the TBIP model performance improved compared to fitting with the lower half. Only six of 19 solutions have an AAD over 0.005 for the TBIP model. We attribute this improvement primarily to the smaller relative uncertainties of the upper half points. In contrast, the NRTL model performance gets worse, failing for ethanol/[HMIM][$(CH_3)_2PO_4$] and water/[EMIM][Tf_2N]. The lowest nine points of ethanol/[HMIM][$(CH_3)_2PO_4$] have deviations larger than 0.06 mol/mol. Besides, a point $x_1 = 0.999$ mol/mol unexpectedly converge to zero, which implies that the NRTL potentially make some erroneous predictions even for conditions that are nominally covered in the correlation. In addition, a quarter of all points of water/[EMIM][Tf_2N] wrongly converge to zero in the NRTL model, while the average absolute deviation for water/[EMIM][Tf_2N] by the TBIP model is only 0.0039 mol/mol.

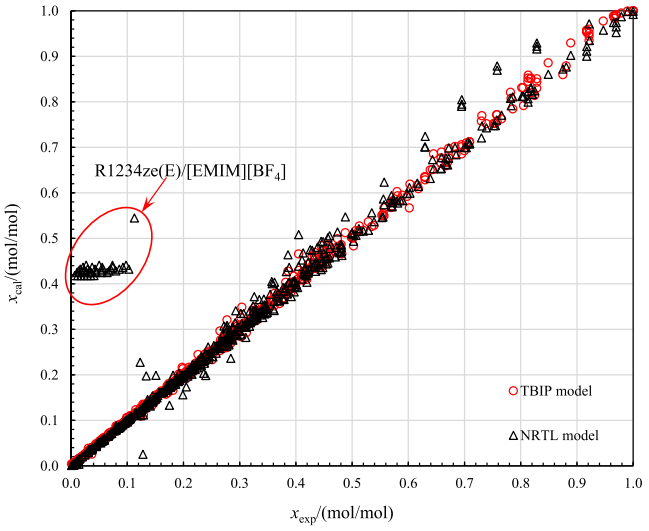

Figure 9. Comparison between experimental data and calculated results when fitting with the lower half points [x (molecular solute) + $(1 - x)$ (ionic liquid)].

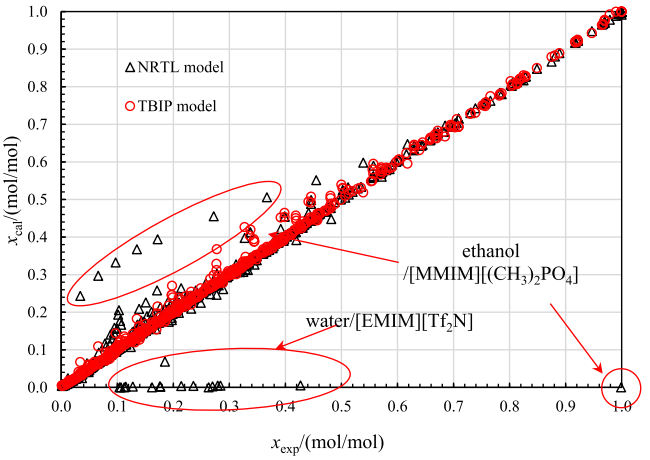

Figure 10. Comparison between experimental data and calculated results when fitting with the upper half solubilities [x (molecular solute) + $(1 - x)$ (ionic liquid)].

7. CONCLUSIONS

A TBIP model was built to cover the thermal effect on excess entropy. Since excess entropy of the solution cannot be explicitly formulated, the excess Gibbs free energy was indirectly calculated from excess internal energy, without losing the excess entropy effect. To adapt with the solutions of monomolecular solute/ionic liquid, the TBIP model considers strong repulsive forces between like-ions together with local electroneutrality assumption to reduce the number of necessary binary−interaction parameters. Additionally, volume elements are introduced to evaluate molecular and ion sizes. As a result, even though monomolecular solute/ionic liquid mixtures are ternary solutions, the necessary number of the parameters for binary energy terms is reduced to only two in comparison with six for the UNIQAC model.

https://doi.org/10.1021/acs.iecr.1c01351
Ind. Eng. Chem. Res. 2021, 60, 11490−11501

When tested against 19 different solutions, the TBIP model has a better performance than the NRTL model, except for water/choline lactate, water/choline glycolate, and ethanol/[MMIM][$(CH_3)_2PO_4$]. We attribute these cases to a low reliability of the available experimental data. When fitted only with the lower half of solubility points, ten of the 19 tested solutions have an AAD over 0.005 for our TBIP model, compared to 14 out of 19 for the NRTL model. Meanwhile, the NRTL model also fails to give accurate predictions for R1234ze(E)/[EMIM][BF_4]. When fitted only with the upper half, the NRTL model fails for both ethanol/[MMIM]-[$(CH_3)_2PO_4$] and water/[emim][Tf_2N], while the TBIP model works much better. Only six of 19 solutions have an AAD over 0.005 for the TBIP model. Therefore, the TBIP model has a good precision and a better robustness in extrapolation and is a valuable and easy-to-use asset for the determination of key thermo-physical property data for solutions containing ionic liquids.

■ ASSOCIATED CONTENT

Supporting Information

The Supporting Information is available free of charge at https://pubs.acs.org/doi/10.1021/acs.iecr.1c01351.

Deviation comparison between the TBIP model and NRTL model (PDF)

■ AUTHOR INFORMATION

Corresponding Author

Maogang He − *Key Laboratory of Thermal Fluid Science and Engineering of MOE, School of Energy and Power Engineering, Xi'an Jiaotong University, Xi'an 710049, China;* orcid.org/0000-0002-4384-4284; Phone: +86-29-8266-3863; Email: mghe@mail.xjtu.edu.cn; Fax: +86-29-8266-3863

Authors

Lihang Bai − *Key Laboratory of Thermal Fluid Science and Engineering of MOE, School of Energy and Power Engineering, Xi'an Jiaotong University, Xi'an 710049, China*

Tao Wang − *Key Laboratory of Thermal Fluid Science and Engineering of MOE, School of Energy and Power Engineering, Xi'an Jiaotong University, Xi'an 710049, China*

Patricia B. Weisensee − *Department of Mechanical Engineering and Materials Science, Washington University in St. Louis, St. Louis, Missouri 63130, United States;* orcid.org/0000-0003-0283-9347

Xiangyang Liu − *Key Laboratory of Thermal Fluid Science and Engineering of MOE, School of Energy and Power Engineering, Xi'an Jiaotong University, Xi'an 710049, China;* orcid.org/0000-0002-8636-1610

Complete contact information is available at: https://pubs.acs.org/10.1021/acs.iecr.1c01351

Notes

The authors declare no competing financial interest.

■ ACKNOWLEDGMENTS

Support by the National Natural Science Foundation of China (no. 51936009 and no. 51721004) and the Program of Introducing Talents of Discipline to Universities (no. B16038) is acknowledged. We also appreciate the support from the Joint Education Program sponsored by the China Scholarship Council (no. 20190628336).

■ REFERENCES

(1) Mathias, P. M. A Versatile Phase Equilibrium Equation of State. *Ind. Eng. Chem. Process Des. Dev.* **1983**, *22*, 385−391.

(2) Ramdharee, S.; Muzenda, E.; Belaid, M. A Review of the Equations of State and Their Applicability in Phase Equilibrium Modeling. *International Conference on Chemical and Environmental Engineering*, 2013; pp 84−87.

(3) Lopez-Echeverry, J. S.; Reif-Acherman, S.; Araujo-Lopez, E. Peng-Robinson Equation of State: 40 Years through Cubics. *Fluid Phase Equilib.* **2017**, *447*, 39−71.

(4) Coutinho, J. A. P. Predictive Local Composition Models: NRTL and UNIQUAC and Their Application to Model Solid−Liquid Equilibrium of n-Alkanes. *Fluid Phase Equilib.* **1999**, *158−160*, 447−457.

(5) Gross, J.; Sadowski, G. Application of the Perturbed-Chain SAFT Equation of State to Associating Systems. *Ind. Eng. Chem. Res.* **2002**, *41*, 5510−5515.

(6) Chen, C.-C.; Evans, L. B. Thermodynamics of Electrolytes. 1. Theoretical Basis and General Equations. *Chem. Eng. Prog.* **1986**, *32*, 444−454.

(7) Pitzer, K. S. *A Thermodynamic Model for Aqueous Solutions of Liquid-like Density*; Lawrence Berkeley National Laboratory, 1987.

(8) Chen, C.-C.; Britt, H. I.; Boston, J. F.; Evans, L. B. Local Composition Model for Excess Gibbs Energy of Electrolyte Systems. Part I: Single Solvent, Single Completely Dissociated Electrolyte Systems. *AIChE J.* **1982**, *28*, 588−596.

(9) Rogers, R. D. *Science* **2003**, *302*, 792−793. Xu, W.; Angell, C. A. *Science* **2003**, *302*, 422−425. Seddon, K. R. *Nat. Mater.* **2003**, *2*, 363−365.

(10) Welton, T. Room-Temperature Ionic Liquids. Solvents for Synthesis and Catalysis. *Chem. Rev.* **1999**, *99*, 2071−2084.

(11) Huddleston, J. G.; Swatloski, R. P.; Rogers, R. D.; Visser, E.; Rogers, D.; Room, R. Temperature Ionic Liquids as Novel Media for 'Clean' Liquid−Liquid Extraction. *Chem. Commun.* **1998**, 1765−1766.

(12) Marsh, K. N.; Deev, A.; Wu, A. C.-T.; Tran, E.; Klamt, A. Room Temperature Ionic Liquids as Replacements for Conventional Solvents − A Review. *Korean J. Chem. Eng.* **2002**, *19*, 357−362.

(13) Zhu, Z.; Xu, Y.; Li, H.; Shen, Y.; Meng, D.; Cui, P.; Ma, Y.; Wang, Y.; Gao, J. Separation of Isopropyl Alcohol and Isopropyl Ether with Ionic Liquids as Extractant Based on Quantum Chemical Calculation and Liquid-Liquid Equilibrium Experiment. *Sep. Purif. Technol.* **2020**, *247*, 116937.

(14) Yang, J.; Hou, Z.; Wen, G.; Cui, P.; Wang, Y.; Gao, J. A Brief Review of the Prediction of Liquid−Liquid Equilibrium of Ternary Systems Containing Ionic Liquids by the COSMO-SAC Model. *J. Solut. Chem.* **2019**, *48*, 1547−1563.

(15) Domańska, U.; Pobudkowska, A.; Królikowski, M. Separation of Aromatic Hydrocarbons from Alkanes Using Ammonium Ionic Liquid C2NTf2 at T= 298.15 K. *Fluid Phase Equilib.* **2007**, *259*, 173−179.

(16) Zhang, J.; Huang, C.; Chen, B.; Ren, P.; Lei, Z. Extraction of Aromatic Hydrocarbons from Aromatic/Aliphatic Mixtures Using Chloroaluminate Room-Temperature Ionic Liquids as Extractants. *Energy Fuels* **2007**, *21*, 1724−1730.

(17) Alonso, L.; Arce, A.; Francisco, M.; Soto, A. Solvent Extraction of Thiophene from N-Alkanes (C7, C12, and C16) Using the Ionic Liquid [C_8mim][BF_4]. *J. Chem. Thermodyn.* **2008**, *40*, 966−972.

(18) Cadena, C.; Anthony, J. L.; Shah, J. K.; Morrow, T. I.; Brennecke, J. F.; Maginn, E. J. Why Is CO2 so Soluble in Imidazolium-Based Ionic Liquids? *J. Am. Chem. Soc.* **2004**, *126*, 5300−5308.

(19) Shiflett, M. B.; Yokozeki, A. Solubility of CO_2 in Room Temperature Ionic Liquid [Hmim][Tf2N]. *J. Phys. Chem. B* **2007**, *111*, 2070−2074.

(20) Wang, Y.; Liu, X.; Kraslawski, A.; Gao, J.; Cui, P. A Novel Process Design for CO_2 Capture and H2S Removal from the Syngas Using Ionic Liquid. *J. Clean. Prod.* **2019**, *213*, 480−490.

(21) Soave, G. Equilibrium Constants from a Modified Redlich-Kwong Equation of State. *Chem. Eng. Sci.* **1972**, *27*, 1197−1203.

(22) Abrams, D. S.; Prausnitz, J. M. Statistical Thermodynamics of Liquid Mixtures: A New Expression for the Excess Gibbs Energy of Partly or Completely Miscible Systems. *AIChE J.* **1975**, *21*, 116−128.
(23) Bai, L.; He, M.; Liu, X.; Ye, Z. A New Activity Coefficient Model for the Solution of Molecular Solute + Ionic Liquid. *Fluid Phase Equilib.* **2019**, *493*, 144−152.
(24) Lyckman, E. W.; Eckert, C. A.; Prausnitz, J. M. Generalized Reference Fugacities for Phase Equilibrium Thermodynamics. *Chem. Eng. Sci.* **1965**, *20*, 685−691.
(25) Rao, V. S.; Krishna, T. V.; Mohan, T. M.; Rao, P. M. Investigations of Molecular Interactions in Binary Mixtures of the Ionic Liquid [Emim][BF_4] and N-Methylaniline at Temperatures from 293.15 to 323.15 K. *J. Solut. Chem.* **2017**, *46*, 281−304.
(26) Zhang, Q.; Feng, S.; Zhang, X.; Wei, Y. Thermodynamic Properties and Intermolecular Interactions of Ionic Liquids [DEME]-[BF_4] or [DEME][TFSI] and Their Binary Mixture Systems with GBL. *J. Mol. Liq.* **2021**, *328*, 115373.
(27) Bhanuprakash, P.; Narasimha Rao, C.; Sivakumar, K. Evaluation of Molecular Interactions by Volumetric and Acoustic Studies in Binary Mixtures of the Ionic Liquid [EMIM][MeSO4] with Ethanoic and Propanoic Acid at Different Temperatures. *J. Mol. Liq.* **2016**, *219*, 79−87.
(28) Maurer, G.; Prausnitz, J. M. On the Derivation and Extension of the Uniquac Equation. *Fluid Phase Equilib.* **1978**, *2*, 91−99.
(29) Huggins, M. L. Some Properties of Solutions of Long-Chain Compounds. *J. Phys. Chem.* **1942**, *46*, 151−158.
(30) Staverman, A. J. The Entropy of High Polymer Solutions. *Recl. Trav. Chim. Pays-Bas* **1950**, *69*, 163−174.
(31) Liu, X.; Bai, L.; Liu, S.; He, M. Vapor−Liquid Equilibrium of R1234yf/[HMIM][Tf2N] and R1234ze (E)/[HMIM][Tf2N] Working Pairs for the Absorption Refrigeration Cycle. *J. Chem. Eng. Data* **2016**, *61*, 3952−3957.
(32) Vapor−Liquid Equilibrium Measurements of Difluoromethane + [Emim]OTf, Difluoromethane + [Bmim]OTf, Difluoroethane + [Emim]OTf, and Difluoroethane + [Bmim]OTf Systems | Journal of Chemical & Engineering Data. https://pubs.acs.org/doi/abs/10.1021/je2005566 (accessed April 07, 2021).
(33) Lemmon, E. W.; Huber, M. L.; McLinden, M. O. Reference Fluid Thermodynamic and Transport Properties-REFPROP Version 8.0. *NIST Standard Reference Database*; NIST, 2007; Vol. 23.
(34) Liu, X.; Lv, N.; Su, C.; He, M. Solubilities of R32, R245fa, R227ea and R236fa in a Phosphonium-Based Ionic Liquid. *J. Mol. Liq.* **2016**, *218*, 525−530.
(35) Neves, C. M. S. S.; Carvalho, P. J.; Freire, M. G.; Coutinho, J. A. P. Thermophysical Properties of Pure and Water-Saturated Tetradecyltrihexylphosphonium-Based Ionic Liquids. *J. Chem. Thermodyn.* **2011**, *43*, 948−957.
(36) Wang, X.; Zhang, Y.; Wang, D.; Sun, Y. Phase Equilibria of Trans-1, 3, 3, 3-Tetrafluoropropene with Three Imidazolium Ionic Liquids. *J. Chem. Eng. Data* **2017**, *62*, 1825−1831.
(37) Gardas, R. L.; Freire, M. G.; Carvalho, P. J.; Marrucho, I. M.; Fonseca, I. M. A.; Ferreira, A. G. M.; Coutinho, J. A. P. High-Pressure Densities and Derived Thermodynamic Properties of Imidazolium-Based Ionic Liquids. *J. Chem. Eng. Data* **2007**, *52*, 80−88.
(38) Liu, X.; Qi, X.; Lv, N.; He, M. Gaseous Absorption of Fluorinated Ethanes by Ionic Liquids. *Fluid Phase Equilib.* **2015**, *405*, 1−6.
(39) Shiflett, M. B.; Harmer, M. A.; Junk, C. P.; Yokozeki, A. Solubility and Diffusivity of Difluoromethane in Room-Temperature Ionic Liquids. *J. Chem. Eng. Data* **2006**, *51*, 483−495.
(40) Watanabe, M.; Kodama, D.; Makino, T.; Kanakubo, M. CO_2 Absorption Properties of Imidazolium Based Ionic Liquids Using a Magnetic Suspension Balance. *Fluid Phase Equilib.* **2016**, *420*, 44−49.
(41) Seki, S.; Tsuzuki, S.; Hayamizu, K.; Umebayashi, Y.; Serizawa, N.; Takei, K.; Miyashiro, H. Comprehensive Refractive Index Property for Room-Temperature Ionic Liquids. *J. Chem. Eng. Data* **2012**, *57*, 2211−2216.
(42) Bhattacharjee, A.; Carvalho, P. J.; Coutinho, J. A. P. The Effect of the Cation Aromaticity upon the Thermophysical Properties of Piperidinium-and Pyridinium-Based Ionic Liquids. *Fluid Phase Equilib.* **2014**, *375*, 80−88.
(43) Yokozeki, A.; Shiflett, M. B. Separation of Carbon Dioxide and Sulfur Dioxide Gases Using Room-Temperature Ionic Liquid [Hmim]-[Tf2N]. *Energy Fuels* **2009**, *23*, 4701−4708.
(44) Kanakubo, M.; Harris, K. R. Density of 1-Butyl-3-Methylimidazolium Bis (Trifluoromethanesulfonyl) Amide and 1-Hexyl-3-Methylimidazolium Bis (Trifluoromethanesulfonyl) Amide over an Extended Pressure Range up to 250 MPa. *J. Chem. Eng. Data* **2015**, *60*, 1408−1418.
(45) Constantinescu, D.; Schaber, K.; Agel, F.; Klingele, M. H.; Schubert, T. J. S. Viscosities, Vapor Pressures, and Excess Enthalpies of Choline Lactate + Water, Choline Glycolate + Water, and Choline Methanesulfonate + Water Systems. *J. Chem. Eng. Data* **2007**, *52*, 1280−1285.
(46) Krannich, M.; Heym, F.; Jess, A. Characterization of Six Hygroscopic Ionic Liquids with Regard to Their Suitability for Gas Dehydration: Density, Viscosity, Thermal and Oxidative Stability, Vapor Pressure, Diffusion Coefficient, and Activity Coefficient of Water. *J. Chem. Eng. Data* **2016**, *61*, 1162−1176.
(47) Machida, H.; Taguchi, R.; Sato, Y.; Smith, R. L., Jr. Measurement and Correlation of High Pressure Densities of Ionic Liquids, 1-Ethyl-3-Methylimidazolium l-Lactate ([Emim][Lactate]), 2-Hydroxyethyl-Trimethylammonium l-Lactate ([$(C_2H_4OH)(CH_3)_3N$][Lactate]), and 1-Butyl-3-Methylimidazolium Chloride ([Bmim][Cl]). *J. Chem. Eng. Data* **2010**, *56*, 923−928.
(48) Hiraga, Y.; Goto, M.; Sato, Y.; Smith, R. L., Jr. Measurement of High Pressure Densities and Atmospheric Pressure Viscosities of Alkyl Phosphate Anion Ionic Liquids and Correlation with the E*-Modified Sanchez-Lacombe Equation of State. *J. Chem. Thermodyn.* **2017**, *104*, 73−81.
(49) Husson, P.; Pison, L.; Jacquemin, J.; Gomes, M. F. C. Influence of Water on the Carbon Dioxide Absorption by 1-Ethyl-3-Methylimidazolium Bis(Trifluoromethylsulfonyl)Amide. *Fluid Phase Equilib.* **2010**, *294*, 98−104.
(50) Rocha, M. A. A.; Neves, C. M. S. S.; Freire, M. G.; Russina, O.; Triolo, A.; Coutinho, J. A. P.; Santos, L. M. N. B. F. Alkylimidazolium Based Ionic Liquids: Impact of Cation Symmetry on Their Nanoscale Structural Organization. *J. Phys. Chem. B* **2013**, *117*, 10889−10897.

https://doi.org/10.1021/acs.iecr.1c01351
Ind. Eng. Chem. Res. 2021, 60, 11490−11501